Chimera complexity

Serhiy Brezetsky[1], Patrycja Jaros[1], Roman Levchenko,[2,3] Tomasz Kapitaniak[1], and Yuri Maistrenko[1,3,4]

[1]*Division of Dynamics, Lodz University of Technology, Stefanowskiego 1/15, 90-924 Lodz, Poland*
[2]*Faculty of Radiophysics, Electronics and Computer Systems, Taras Shevchenko National University of Kyiv,
Volodymyrska St. 60, 01030 Kyiv, Ukraine*
[3]*Forschungszentrum Jülich, 52428 Jülich, Germany*
[4]*Institute of Mathematics and Centre for Medical and Biotechnical Research, NAS of Ukraine, Tereshchenkivska St. 3, 01030 Kyiv, Ukraine*

We show an amazing complexity of the chimeras in small networks of coupled phase oscillators with inertia. The network behavior is characterized by heteroclinic switching between multiple saddle chimera states and riddling basins of attractions, causing an extreme sensitivity to initial conditions and parameters. Additional uncertainty is induced by the presumable coexistence of stable phase-locked states or other stable chimeras as the switching trajectories can eventually tend to them. The system dynamics becomes hardly predictable, while its complexity represents a challenge in the network sciences.

Chimera states represent a fast growing research branch of nonlinear science, which aims to understand how a network of identical oscillators can split into groups with essentially different behavior, such as one group being regular and the other chaotic [1,2]. Currently, we observe a tremendous activity in this area leading to a number of theoretical and experimental studies (see the review papers [3–6] and references therein). In real-world systems, chimera states may play a role in the understanding of peculiar complex behaviors in biological [7–10], engineering [11–16], and social [17] systems.

In 2015, Ashwin and Burylko defined a new type of chimera behavior, called the *weak* chimera state, which allowed to derive chimeras in small networks of coupled phase oscillators. According to the definition, in a weak chimera state at least one oscillator should rotate with a different average frequency (Poincaré winding number) in comparison to at least two others which are frequency synchronized. First, the weak chimera states were reported for four phase oscillators with the Hansel-Mato-Meunier (HMM) coupling, i.e., coupled through the first two harmonics [18–20], and for three Kutamoto-Sakaguchi equations with inertia [21]. Experimentally, they have been obtained in small networks of coupled semiconductor lasers [22] and optoelectronic oscillators [23], and in coupled mechanical oscillators (metronomes) [24]. So-called solitary states develop when only one or a few oscillators split up from the main synchronized cluster and start to rotate in a different manner. Representing a subclass of weak chimeras, solitary states are qualitatively different from the "classical" chimeras discovered in [1,2], typically arising not only in small but also in fine-sized networks [25], in the mean-field limit [26], and in adaptive systems [27].

Heteroclinic switching between chimera states was first reported in [21] for $N = 3$ mean-field coupled phase oscillators with inertia [28] of the general form

$$m\ddot{\theta}_i + \varepsilon\dot{\theta}_i = \omega + \frac{\mu}{N}\sum_{j=1}^{N}\sin(\theta_j - \theta_i - \alpha). \quad (1)$$

Here θ_i ($i = 1, \ldots, N$) are phase variables, α is a phase lag, and μ is a coupling strength. Other parameters m, ε, and ω are mass, damping, and natural frequency of a single oscillator (pendulum). We put $m = 1.0$, $\varepsilon = 0.1$, and $\omega = 0$. The switching is obtained as a result of a loss of stability of chimera states transforming thus into the chaotic saddles. For the $N = 3$ case, it develops in narrow layers close to the boundaries of the chimera regions (see Chap. S4 of the Supplemental Material [29] for details). In [30], the heteroclinic switching between chimeras was reported for small networks, beginning from $N = 6$ phase oscillators with the HMM coupling. In [31] an example of this kind of behavior was analyzed for the $N = 7$ case of model (1), and in [32] for a model of coupled logistic maps. The importance of riddled [33] and intermingled [34] basins of attraction in the context of chimera states was pointed out in [32,35].

In this Letter, we discuss the chaotic chimera switching phenomenon in model (1) with $N = 4$ and $N = 5$. The complexity of the system behavior is illustrated in Fig. 1, where basins of attraction of the chimera states are shown manifesting a microscopic, visually riddled basin structure. Typical switching trajectories are shown in the upper panel, where chimeras with one and two splitted oscillators participating in the switching can be recognized. The system dynamics is characterized by an extreme sensitivity to the initial conditions and the parameters, with precise trajectory behavior becoming hardly predictable. Additional uncertainty for the $N = 4$ case is induced by stable phase-locked states, always coexisting with the chimera states (see Chap. S2 of the Supplemental
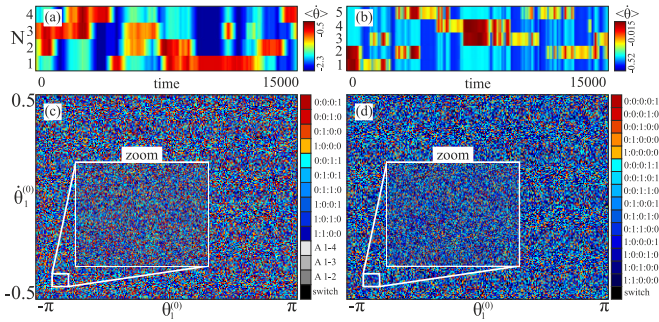
FIG. 1. Heteroclinic switching between chimera states (a),(b) and basins of attraction (c),(d) for network (1) with $N = 4$ (left panel) and $N = 5$ (right panel). The basins are built in the grid plane $(\theta_1^{(0)}, \dot{\theta}_1^{(0)})$ by fixing the initial conditions of the remaining oscillators (see detail in [36]). Color gamma indicates different chimera states (colored), phase-locked states (gray), and the switching behavior (black). The insets in (c) and (d) show zooms of the small grid square to confirm the microscopic basin structure. Parameters: $\mu = 0.3$, $\alpha = 1.59$ ($N = 4$) and $\mu = 0.054$, $\alpha = 1.67$ ($N = 5$).

Material [29] for details); then the switching dynamics is mostly transient. The situation is different for model (1) with $N = 5$: There is no stable phase-locked state in the region of interest, and the switching behavior is perpetual. We expect that this kind of intricate collective dynamics in small dimensions may be a precursor to *spatial chaos* [37] for bigger networks of this type discussed recently in [25].

To clarify the mechanism of the chaotic switching phenomenon, consider first Eq. (1) with $N = 4$. Results of direct numerical simulation in the two-parameter plane of the phase lag α and coupling strength μ are presented in Fig. 2. This figure reveals the appearance of three principal chimera regions for in-phase, antiphase, and rotating wave chimera states
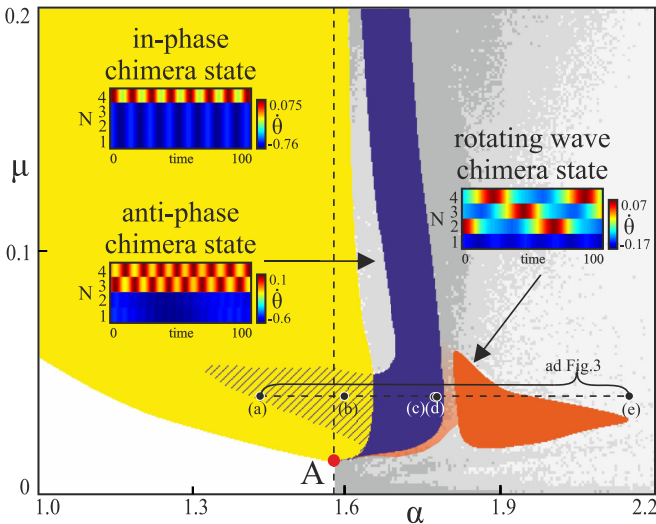

FIG. 2. Regions of chimera states for model (1) with $N = 4$ in the (α, μ) parameter plane with winding numbers (1;0;0;0), (1;1;0;0), and (1;1;1;0). Typical frequency plots are shown in the insets. Gray shaded regions correspond to transient switching behavior. The parameter point ($\mu = 0.3$, $\alpha = 1.59$) for Figs. 1(a) and 1(c) lies between the yellow and blue regions above the range shown.

symbolically denoted as (1;0;0;0), (1;1;0;0), and (1;1;1;0). The regions resemble Arnold tongues issued from a singular parameter point $A(\alpha = \pi/2, \mu \approx 0.01406)$ in which a transcritical-pitchfork bifurcation of the synchronous state meets with a homoclinic bifurcation at the lower edge curve of the in-phase chimera region (see Chap. S1 of the Supplemental Material [29] for details). Note that two chimera regions, in phase (1:0:0:0) and antiphase, (1:1:0:0), intersect through the dashed subregion, where four chimeras of the first type (1;0;0;0) and six of the second (1;1;0;0) coexist. Chimera basins can gain in this case an involved fine-grained structure illustrated in Fig. 1(c), which is despite the Lyapunov stability of each of the ten existing chimera states.

An additional complexity of the dynamics is induced by the so-called antipodal points which are stable equilibria of Eq. (1) with $N = 4$ coexisting with the chimeras at any $\alpha > \pi/2$ [gray basins in Fig. 1(c)]. The antipodal phase configuration means that two oscillator pairs stay in the antiphase and are shifted by an arbitrary angle β with respect to each other, i.e.,

$$\theta_1 = \gamma, \ \theta_2 = \gamma + \beta, \ \theta_3 = \gamma + \pi, \ \theta_4 = \gamma + \beta + \pi. \quad (2)$$

The antiphase pairs coincide at $\beta = 0$ and split up for $\beta > 0$ reaching eventually the symmetric splay state at $\beta = \pi/2$. To explore the stability of the phase-locked states in Eq. (1) with $N = 4$, let us rewrite it in an equivalent form of only three equations in phase differences $\eta_i = \theta_i - \theta_4$, $i \in \{1, 2, 3\}$:

$$m\ddot{\eta}_i + \varepsilon\dot{\eta}_i = \frac{\mu}{4}(\sin(\eta_{i+1} - \eta_i - \alpha) + \sin(-\eta_i - \alpha)$$

$$+ \sin(\eta_{i+1} - \eta_i - \alpha) - \sum_{j=-1}^{1} \sin(\eta_{i+j} - \alpha)).$$

$$(3)$$

The in-phase synchronous state ($\theta_1 = \theta_2 = \theta_3 = \theta_4$) turns into the trivial fixed point $O(\eta_i = \dot{\eta}_i \equiv 0)$. Its eigenvalues are $\lambda_{1-6} = (-\varepsilon \pm \sqrt{\varepsilon^2 - 4\mu\cos\alpha})/2$, which implies that O is stable at any $\alpha < \pi/2$ and unstable at any $\alpha > \pi/2$, valid for any $\mu > 0$. For model (1), O represents the synchronous in-phase state of a constant velocity $\dot{\theta}_{1-4} = -\mu/\varepsilon \sin\alpha$.

The antipodal fixed points (2) create a one-dimensional manifold in the phase space of Eq. (3): $M \equiv \{\eta_1 = \beta, \ \eta_2 = \pi, \ \eta_3 = \pi + \beta; \ \beta \in [0; \pi/2]\}$ with the eigenvalues $\lambda_1 = -\varepsilon$, $\lambda_2 = 0$, and $\lambda_{3-6} = -(\varepsilon \pm \sqrt{\varepsilon^2 + 2\mu\cos\alpha \pm 2\mu\sqrt{\cos^2\alpha - \sin^2\beta}})/2$. It implies that the antipodal states are stable for $\alpha < \pi/2$ under the condition $\mu < 2\varepsilon^2\cos\alpha/(\cos^2\alpha - \sin^2\beta)$ at $\alpha \in (\pi/2, \pi/2 + \beta)$ and for any $\mu > 0$ at $\alpha \in (\pi/2 + \beta, \pi)$, and they are unstable at $\alpha < \pi/2$. The state with $\beta = 0$ (two antiphase pairs coincide) is stable for any $\alpha > \pi/2$ and $\mu > 0$; stability regions of the others shrink gradually with an increase of β (see Chap. S2 of the Supplemental Material [29] for details).

We conclude that stable phase-locked states are unavoidable in model (1) for the $N = 4$ case, no matter what parameters are chosen. They are the in-phase synchronous state at $\alpha < \pi/2$ and a continuum of the antipodal states at $\alpha > \pi/2$. Because of that, the switching behavior has a transient character, observed in the so-called riddling shadows surrounding the chimera regions, shown in gray. More
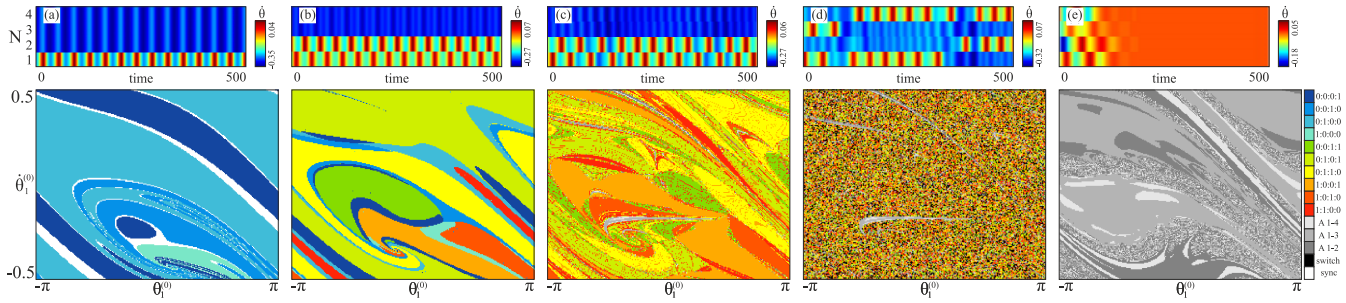
FIG. 3. Basin switching transition in model (1) with $N = 4$ for fixed coupling strength $\mu = 0.04$ (black dots in Fig. 2). For each value of the phase lag parameter α (increasing from left to right, $\alpha = 1.43$, 1.6, 1.775, 1.78, and 2.15, respectively), basins (bottom panel) and typical solutions (top panel) are shown (see [36,40] for details).

saturated areas correspond to the longer lifetime for a typical switching trajectory before it collapses in an antipodal state. Our simulations confirm that the chimera switching can be terminated in any unpredictable moment of time, after a short or long transient, with a sensitive dependence on the initial conditions, system, and simulation parameters. The global co-existence of stable trivial states causes even more puzzling in the chaotic switching dynamics of model (1). It is imposed by an additional symmetry of the networks with even N [which is not the case for Eq. (1) with $N = 5$ as below].

To finalize the $N = 4$ case, we present a typical scenario for the multistable basin transition, illustrated in Fig. 3. We fix the coupling strength $\mu = 0.04$ and increase the phase lag parameter α along the horizontal line with dots in Fig. 2. First, in Fig. 3(a), the basin structure is relatively simple for $\alpha = 1.43$. Thus, the parameter point lies inside the (1;0;0;0)-chimera region such that the basin contains four shades of blue corresponding to four permutationally different chimeras of this type. Additional tiny blank areas mark full synchronization. With an increase of α, new red, yellow, and green shades appear, manifesting the (1;1;0;0)-type chimeras, ten in total [Fig. 3(b), $\alpha = 1.6$]. Soon after, (1;0;0;0)-type stable chimeras become saddles, and the basin acquires a clear sign of fractality [Fig. 3(c), $\alpha = 1.775$]. Slightly beyond, the basin is microscopic and visually riddled [Fig. 3(d), $\alpha = 1.78$], although the (1:1:0:0) chimeras are still stable. They transform in saddles with further increase of α, while the basin becomes totally riddled with the antipodal states described above. The system behavior typically develops then in the form of heteroclinic switching between all existing saddle chimera states. This is valid with further increase of α until the next, rotating chimera region shown in brick red color (Fig. 2). After, the switching lifetime decreases, and all initial points result in antipodal states of different configurations, as illustrated in Fig. 3(e) ($\alpha = 2.15$).

In model (1) with $N = 5$, on the contrary, there are no stable phase-locked states in the parameter region of interest at $\alpha > \pi/2$. The chimera switching behavior becomes then persistent, unavoidable under perturbations. Figure 4 illustrates how the switching arises in the parameter gap between the two chimera regions: one to the left (shown in light blue) is for chaotic chimeras of the type (1:1:0:0:0), and the second to the right (shown in light red) for the so-called antipodal chimera states of the type (1:1:1:1:0).

The mechanism of the switching transition in this case includes riddling and blowout bifurcations [41]. Consider a chaotic chimera trajectory for parameters inside the (1:1:0:0:0) region. Its behavior is characterized by three identically equal oscillators [see inset in Fig. 4(a)]; i.e., it is reduced to an invariant manifold of the form $M \equiv \{\theta_1 = \theta_2 = \theta_3\}$. In the manifold, the dynamics is governed by a chaotic attractor $A \subset M$ with one positive Lyapunov exponent $\lambda_{in} > 0$ [see graph in Fig. 4(b)]. The switchings arise in a riddling bifurcation, when an unstable periodic orbit Q embedded in the in-manifold attractor A loses transverse stability, while the attractor itself remains transversely stable on average [given by the condition $\lambda_{tr}(A) < 0$]. Fixing $\mu = 0.1$, we find that this happens at $\alpha_r \approx 1.6236$ [cf. dashed line in Fig. 4(b)]. Beyond the riddling bifurcation, small errors in the solution behavior (due to the algorithm precision) can induce sudden jumps of the trajectory out of the manifold M. This occurs when the trajectory passes close to the unstable periodic orbit Q, shown in Fig. 4(c), and lingers there for a time sufficient for getting a required amount of transverse repelling from M. After a relatively short transient motion from the manifold, the trajectory comes again close to one of the chimera manifolds [in total, there are $\binom{5}{2} = 10$ permutationally identical copies of them]. The situation is repeated, producing the switching events one after another. Our simulations show [see Fig. 4(d)] that the average switching period T follows then the superexponential law

$$T \sim \exp[K(\alpha - \alpha_r)^{-2/3}], \qquad (4)$$

and $K > 0$ is a constant. It is similar to the asymptotic properties of riddling bifurcation in terms of a symmetry-breaking control parameter [42].

The blowout bifurcation occurs when two coinciding transverse Lyapunov exponents $\lambda_{tr}(A)$ of the attractor A become positive; for the parameters in Figs. 4(b)–4(e) it happens at $\alpha_b \approx 1.6425$. A transforms into a Milnor attractor [43], which means that it attracts only a positive (but not the full) measure set of points from any of its neighborhood in the whole phase space. Beyond the blowout bifurcation the average switching period T decreases more slowly; note a break point in Fig. 4(d) in the blowout moment.

The next change for the chimera switching transition occurs at $\alpha_Q \approx 1.6471$, when the periodic orbit $Q \in A$ (responsible for the onset of switching in the riddling bifurcation)
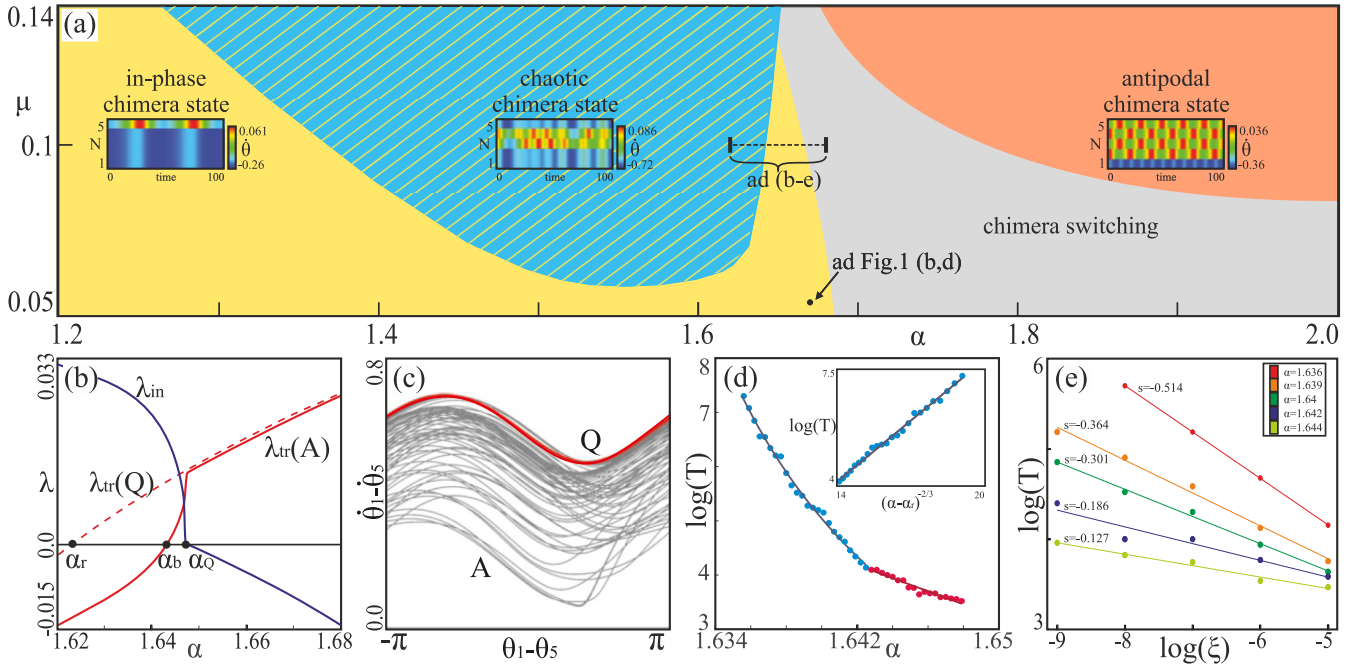
FIG. 4. (a) Chimera regions for model (1) with $N = 5$ in the (α, μ) parameter plane; (b)–(e) parameters belong to the dashed line shown at $\mu = 0.1$. (b) Five largest Lyapunov exponents and transverse Lyapunov exponent $\lambda_{tr}(Q)$ of the in-manifold cycle Q (dashed line). (c) The in-manifold M dynamics, including chaotic attractor A (gray) and unstable periodic orbit Q (red) in the phase difference variables at $\alpha = 1.645$. (d) Averaged switching period T versus α in logarithmic scale; blue and red dots stand for α before and after the blowout bifurcation, respectively; the superexponential scaling law for T versus α is confirmed by a plot in the inset. (e) T versus noise intensity ξ in log-log scale for five chosen values of α between riddling and blowout bifurcations; the numbers indicate scaling exponents of the power law obtained.

inherits the in-manifold M stability. The attractor $A \subset M$ transforms into a chaotic saddle, and the in-manifold behavior represents then a chaotic transient ending eventually in Q. The full system trajectories cannot, however, reach the orbit Q as it is strongly repelling transversely. After approaching Q at a some distance, they go away in the transverse direction and fall down into a switching event. With the further increase of α, the average switching period T gradually decreases, from a few thousandths to a few hundredths until the parameter point meets the antipodal chimera region [see Fig. 4(a)].

A peculiarity of the switching behavior at the final stage of the transition at $\alpha > 1.65$ consists of a gradual swelling of the transitional time intervals, and then the trajectory wanders in a chaotic manner away from the chimera manifolds. The transitional switching intervals (practically infinitesimal soon after the riddling bifurcation) become now comparable in length with the chimeric laps. The solution behavior manifests in this case the so-called laminar-turbulent dynamics. Quantitatively, it is characterized by the turbulent fraction F as the relative part of the transitional behavior. We observe that F grows with α reaching eventually the values greater than 0.5 at $\alpha \approx 1.78$, when the parameter point enters the antipodal chimera region. For larger α the switching behavior becomes transient, and ceases to exist with further increase of α (see Chap. S3 of the Supplemental Material [29] for details).

The important characteristic of the considered network dynamics consists of the presumable coexistence of the switching behavior reported with the other stable chimera states, which makes the system behavior even more mysterious.

To illustrate this, note that the considered parameter interval of the switching transition at $\mu = 0.1$, shown in Fig. 4(a), intersects the region of the in-phase chimera state up to $\alpha \approx 1.67$ and alternatively, with the stable antipodal chimera state beginning from $\alpha \approx 1.78$. These stable chimera states play the role of traps, which can capture the switching solutions after some transient time. Our simulations up to 3×10^7 time units reveal that this takes place for about 10% of the switching solutions, when simulated at the α interval between the riddling and blowout bifurcations. On the other hand, we find that the nontransient, never-ending switching behavior is generic for $1.67 < \alpha < 1.78$, where no other stable states exist in the system phase space [44].

Our last comment concerns the influence of noise on the switching dynamics reported. Results of direct numerical simulations with uniform additive noise incorporated into model (1) with $N = 5$ are presented in Fig. 4(e). It reveals that the average switching period T decreases in a power law with an increase of the noise intensity ξ. The power law obtained confirms the results from [32], which were obtained for another type of system of two-group coupled logistic maps. A difference from our case is that for the maps the average switching period T grows up to minimal noise intensities of the order 10^{-15}. In our case, the values of T saturate at the noise intensities $\sim 10^{-10}$ (not shown in the figure), due to the simulation errors when integrating Eq. (1) (see Chap. S5 of the Supplemental Material [29] for details). It has also to be noticed that the noise applied affects essentially the onset of switching. Without noise the first switching event was detected at $\alpha = 1.6351$ ($\mu = 0.1$ as in Fig. 4; repetitive

simulations with random initial conditions up to $t = 2 \times 10^7$ time units), which is quite far from the precise riddling bifurcation value $\alpha_r \approx 1.6236$. With increase of noise, however, the onset of switching shifted to the riddling bifurcation value, reaching it at $\xi \sim 10^{-5}$.

In conclusion, we have identified a mechanism for the chimera switching transition in networks of coupled oscillators with inertia. The switching has a heteroclinic character and arises when the chimera states lose stability, transforming into saddle states. Onset of the switching is determined by the riddling bifurcation and the noise applied. Chimera basins become riddled and, moreover, intermingled, causing the extreme sensitivity and unpredictability of the system dynamics. Any small uncertainties, either in the initial conditions or system parameters, or even the integration step or algorithm can throw the trajectory into another, totally different itinerary. The pronounced switching has, furthermore, a form of laminar-turbulent behavior, where the chaotic transitional intervals swell to compete with the switching chimera laps. The switching dynamics becomes even more tangled due to its possible coexistence with other stable chimeras or phase-locked states. In the even $N = 4$ case, they are antipodal equilibria causing therefore the transient character of the switching solutions at $\alpha > \pi/2$. In the odd case, $N = 5$, as no such states exist, the switching becomes persistent and never terminating in rather extended regions of the system parameters. It is also robust when incorporating the noise. We expect that the amazing chimera complexity uncovered indicates a common, probably universal phenomenon in the networks of coupled oscillators of very different nature, due to the influence of inertia.

[1] Y. Kuramoto and D. Battogtokh, Nonlinear Phenom. Complex Syst. **5**, 380 (2002).

[2] D. M. Abrams and S. H. Strogatz, Phys. Rev. Lett. **93**, 174102 (2004).

[3] M. J. Panaggio and D. M. Abrams, Nonlinearity **28**, R67 (2015).

[4] E. Schöll, Eur. Phys. J. Spec. Top. **225**, 891 (2016).

[5] O. Omel'chenko and E. Knobloch, New J. Phys. **21**, 093034 (2019).

[6] F. Parastesh, S. Jafari, H. Azarnoush, Z. Shahriari, Z. Wang, S. Boccaletti, and M. Perc, Phys. Rep. **898**, 1 (2021).

[7] J. Hizanidis, N. E. Kouvaris, G. Zamora-Lopez, A. Diaz-Guilera, and C. Antopoulos, Sci. Rep. **6**, 19845 (2016).

[8] N. C. Rattenborg, C. J. Amlaner, and S. L. Lima, Neurosci. Biobehav. Rev. **24**, 817 (2000).

[9] A. Rothkegel and K. Lehnertz, New J. Phys. **16**, 0055006 (2014).

[10] C. Bick, M. Goodfellow, C. R. Laing, and E. A. Martens, J. Math. Neurosci. **10**, 9 (2020).

[11] A. E. Motter, S. A. Myers, M. Angel, and T. Nishikawa, Nat. Phys. **9**, 191 (2013).

[12] L. M. Pecora F. Sorrentino, A. Hagerstrom, T. Murphy, and R. Roy, Nat. Commun. **5**, 4079 (2014).

[13] N. Lazarides and G. Tsironis, Phys. Rep. **752**, 1 (2018).

[14] I. Belykh, R. Jeter, and V. Belykh, Sci. Adv. **3**, e1701512 (2017).

[15] J. Hart, L. Larger, T. Murphy, and R. Roy, Philos. Trans. R. Soc. A **377**, 20180123 (2019).

[16] F. Hellmann, P. Schultz, P. Jaros, R. Levchenko, T. Kapitaniak, and J. Kurths, Nat. Commun. **11**, 592 (2020).

[17] J. C. Gonzales-Avella, M. G. Cosenza, and M. S. Miguel, Physica A **399**, 24 (2014); A. Pikovsky, Math. Model. Nat. Phenom. **16**, 15 (2021).

[18] P. Ashwin and O. Burylko, Chaos **25**, 013106 (2015).

[19] M. J. Panaggio, D. M. Abrams, P. Ashwin, and C. R. Laing, Phys. Rev. E **93**, 012218 (2016).

[20] C. Bick and P. Aswin, Nonlinearity **29**, 1468 (2016).

[21] Y. Maistrenko, S. Brezetsky, P. Jaros, R. Levchenko, and T. Kapitaniak, Phys. Rev. E **95**, 010203(R) (2017).

[22] F. Bohm, A. Zakharova, E. Scholl, and K. Ludge, Phys. Rev. E **91**, 040901(R) (2015); A. Röhm, F. Böhm, and K. Ludge, *ibid.* **94**, 042204 (2016).

[23] J. D. Hart, K. Bansal, T. E. Murphy, and R. Roy, Chaos **26**, 094801 (2016).

[24] J. Wojewoda, K. Czolczynski, Y. Maistrenko, and T. Kapitaniak, Sci. Rep. **6**, 34329 (2016); P. Ebrahimzadeh, M. Schiek, P. Jaros, T. Kapitaniak, S. van Waasen, and Y. Maistrenko, Eur. Phys. J. Spec. Top. **229**, 2205 (2020).

[25] P. Jaros, Y. Maistrenko, and T. Kapitaniak, Phys. Rev. E **91**, 022907 (2015); P. Jaros, S. Brezetsky, R. Levchenko, D. Dudkowski, T. Kapitaniak, and Yu. Maistrenko, Chaos **28**, 011103 (2018).

[26] N. Kruk, Yu. Maistrenko, and H. Koeppl, Chaos **30**, 111104 (2020).

[27] R. Berner, A. Polanska, E. Schöll, and S. Yanchuk, Eur. Phys. J. Spec. Top. **229**, 2183 (2020).

[28] B. Ermentrout, J. Math. Biol. **29**, 571 (1991); H. A. Tanaka, A. J. Lichtenberg, and S. Oishi, Phys. Rev. Lett. **78**, 2104 (1997); S. Olmi, A. Navas, S. Boccaletti, and A. Torcini, Phys. Rev. E **90**, 042905 (2014).

[29] See Supplemental Material at http://link.aps.org/supplemental/10.1103/PhysRevE.103.L050204: Chap. S1, Arnold tongue structure of the chimera regions in the $N = 4$ case; Chap. S2, stability of phase-locked states in the $N = 4$ case; Chap. S3, switching chimera transition in the $N = 5$ case; Chap. S4, heteroclinic switching in the $N = 3$ case; and Chap. S5, simulation algorithm, and influence of noise.

[30] C. Bick, Phys. Rev. E **97**, 050201(R) (2018).

[31] R. J. Goldschmidt, A. Pikovsky, and A. Politi, Chaos **29**, 071101 (2019).

[32] Y. Zhang, Z. G. Nicolaou, J. D. Hart, R. Roy, and A. E. Motter, Phys. Rev. X **10**, 011044 (2020).

[33] J. Alexander, J. Yorke, Z. You, and I. Kan, Int. J. Bifurcation Chaos Appl. Sci. Eng. **2**, 795 (1992).

[34] Y.-C. Lai and C. Grebogi, Phys. Rev. E **52**, R3313(R) (1995).

[35] V. Santos, J. Szezech, A. Batista, K. Iarosz, M. Baptista, H. Ren, C. Grebogi, R. Viana, I. Caldas, Y. Maistrenko, and J. Kurths, Chaos **28**, 081105 (2018).

[36] The macroscopic basins are obtained for the grid plane $(\theta_1^{(0)}, \dot{\theta}_1^{(0)})$ and with fixed initial conditions the other oscillators. Figure 1(c): $\theta_2^{(0)} = 0.88$, $\dot{\theta}_2^{(0)} = -0.18$, $\theta_3^{(0)} = 1.58$, $\dot{\theta}_3^{(0)} = 0.07$, $\theta_4^{(0)} = 1.05$, and $\dot{\theta}_4^{(0)} = 0.07$. Figure 1(d): $\theta_2^{(0)} = 5.54$, $\dot{\theta}_2^{(0)} = -0.43$, $\theta_3^{(0)} = 3.52$, $\dot{\theta}_3^{(0)} = -0.25$, $\theta_4^{(0)} = 5.86$, $\dot{\theta}_4^{(0)} = -0.11$, $\theta_5^{(0)} = 3.72$, and $\dot{\theta}_5^{(0)} = 0.15$. In each point of the $(\theta_1^{(0)}, \dot{\theta}_1^{(0)})$ grid the simulation was performed up to 4000 time units with the first 3800 discarded as a transient, and the last 200 were used for the analysis of the behavior obtained. Our simulations confirm that changing the fixed initial conditions and the simulation parameters does not affect (qualitatively) the developing microscopic structure of the basins.

[37] Spatial chaos means that the number of coexisting stable states grows exponentially fast with the network size N; see [38] and reference therein. In the context of chimera states, spatial chaos was discussed in [39].

[38] P. Coullet, C. Elphick, and D. Repaux, Phys. Rev. Lett. **58**, 431 (1987); S. N. Chow and J. Mallet-Paret, IEEE Trans. Circuits Syst. I **42**, 746 (1995); L. P. Nizhnik, I. L. Nizhnik, and M. Hasler, Int. J. Bifurcation Chaos Appl. Sci. Eng. **12**, 261 (2002).

[39] I. Omelchenko, Y. Maistrenko, P. Hövel, and E. Schöll, Phys. Rev. Lett. **106**, 234102 (2011).

[40] Nonvaried initial conditions for basins in Fig. 3: $\theta_2^{(0)} = 0.88$, $\dot{\theta}_2^{(0)} = -0.18$, $\theta_3^{(0)} = 1.58$, $\dot{\theta}_3^{(0)} = 0.07$, $\theta_4^{(0)} = 1.05$, and $\dot{\theta}_4^{(0)} = 0.07$.

[41] P. Ashwin, J. Buescu, and I. N. Stewart, Phys. Lett. A **193**, 126 (1994); E. Ott, J. Alexander, I. Kan, J. Sommerer, and J. Yorke, Physica D **76**, 384 (1994); E. Ott and J. Sommerer, Phys. Lett. A **188**, 39 (1994); L. Pecora and T. Carroll, Chaos **25**, 097611 (2015).

[42] Y. C. Lai, C. Grebogi, J. A. Yorke, and S. C. Venkataramani, Phys. Rev. Lett. **77**, 55 (1996).

[43] J. Milnor, Commun. Math. Phys. **99**, 177 (1985).

[44] We exclude from the consideration the situation when the switching trajectory is attracted by one of the long periodic orbits (in a neighborhood of a heteroclinic contour) presumably coexisting with the switching behavior. Their basins are normally negligibly small; however, some of them can be characterized by visible windows of stability. See [21], where this phenomenon was discussed in the $N = 3$ case.